Optimization of plotter printing for sub-terahertz metallic metasurfaces fabrication on ultra-thin substrate

Cyprien Brulon, Baptiste Fix, Arthur Salmon, Patrick Bouchon

Optimization of plotter printing for sub-terahertz metallic metasurfaces fabrication on ultra-thin substrate.

Cyprien Brulon[1], Baptiste Fix[1], Arthur Salmon[1], Patrick Bouchon[1]

[1]DOTA, ONERA, Université Paris-Saclay, 91123 Palaiseau, France
*corresponding author, E-mail: cyprien.brulon@onera.fr

Abstract

Additive manufacturing processes have emerged as a promising way to conceive terahertz and millimetric components. In this work, we discuss a printing process for sub-terahertz metallic metasurfaces fabrication on ultra-thin substrates. We demonstrate the use of a plastic substrate with a micrometric thickness which makes this printing method a promising and low cost alternative to conventional optical lithography for the fabrication of flexible terahertz 2D metasurfaces. After detailing the key parameters and limitations, we applied the optimized process to fabricate samples composed of periodic arrays of split ring resonators on 50 µm thick fused silica and 3 µm thick PET substrates. The optical response in transmission of the metasurfaces shows expected resonances in the 100 GHz range and demonstrates the use of microplotter system for rapid prototyping of low-loss terahertz passive components on ultra-thin substrate.

1. Introduction

Technological development in the terahertz (THz) domain (0.1 to 10.0 THz) has accelerated significantly in recent years due to the numerous prospects for applications in various fields such as security, non-destructive testing, medical imaging, molecular spectroscopy and telecommunications, etc [1, 2, 3, 4]. In that perspective, it has been shown that the artificial optical properties of metamaterials can be tailored to design a wide range of terahertz components such as metalenses [5, 6], filters [7, 8, 9], polarizers [10, 11], switches [12, 13, 14, 15], absorbers [16, 17, 18] and isolators [19]. Additive manufacturing techniques have emerged in recent years as a promising alternative to conventional clean room approaches [20, 21, 22]. For three-dimensional structures, stereolithography [23] or fused deposition modeling [24] thus complement computer numerical control machining [25, 26] or laser machining techniques [27]. For two-dimensional terahertz metasurfaces, since the structures of interest are relatively large (millimetre and sub-millimetre), it is possible to replace conventional photolithography processes with printing methods [28, 29, 30, 31, 32]. These allow the fabrication of metallic or dielectric patterns on a decimeter scale while maintaining micrometric fabrication accuracy. In addition to being relatively simple, fast and low-cost, the flexibility of these methods allows the use of a wide variety of substrates such as semiconductors, glasses but also thin polymers and smooth substrates. However, for the fabrication of metallic metasurfaces, two major issues may limit the use of such a technique: on the one hand, the spatial resolution of the printing system fixes the upper accessible frequency and on the other hand, the metal thickness and conductivity -compared with skin depth- sets the lower frequency limit [33]. In recent years, the main systems used are inkjet printers developed for printed electronics [34, 35, 36, 37]. These systems use the pressure exerted by the piezoelectric element on the ink contained in a narrow channel to overcome capillary forces, causing the fluid to be ejected onto a surface in the form of droplets. These printers require the use of relatively low viscosity inks (8-12 cP) and face many challenges such as unwanted generation of satellite drops, splashing or jet control, stability and precision. This standard technology allows resolutions of the order of 50 µm to be achieved with an average deposited thickness of 150-200 nm in a single pass. To increase the resolution, electrodynamic or electrohydrodynamic jet printing [38, 39, 40, 41] or aerosol jet printing [42, 43, 44] have been developed. They allow the resolution to reach the micrometer range, but this is at the expense of the deposited thickness.

In this study we optimize the use of an ultrasonic excited printing system (Microplotter) [45, 46, 47, 48, 49, 50, 51, 52, 33] for metallic ink with a compromise between spatial resolution and thickness. Besides, we demonstrate its application to the fabrication of sub-terahertz metasurfaces. The key printing parameters, such as the tip shape, the ink viscosity, the substrate type, the tip excitation and the printing speed are investigated. Since the ink deposition occurs by contact, the use of more viscous inks is possible, resulting in thicker deposited metal layers. We also show the possibility to further increase the metal thickness by multiple printing passes while maintaining a good spatial resolution. Eventually, we demonstrate the use of the microplotter for the fabrication of sub-terahertz metal metasurfaces on thin substrates, which are subsequently characterized.

2. Microplotter technology/Method

The printing method, based on a Microplotter II (Sonoplot), is illustrated in figure 1. The ink is ejected through a quartz

micropipette brought in contact with the substrate. It is loaded with solution by capillary force when dipped into a reservoir. The approach of the tip is then carried out automatically: the contact with the substrate is detected by an offset of the capillary resonance frequency measured by a piezoelectric element attached to the tip. The latter imposes an ultrasonic excitation under an electric voltage and a vibration of the tip at the frequency of 450 kHz resulting in a continuous release of the ink. The piezo itself is attached to a set of three precision positioning stages that move the tip along a predefined pattern (max speed 100 mm/s) with a lateral positioning error of approximately 1 µm over an area as large as 35 x 30 cm. The whole process is monitored in real time using an integrated CCD camera equipped with a 0.44 NA objective (InfiniStix).

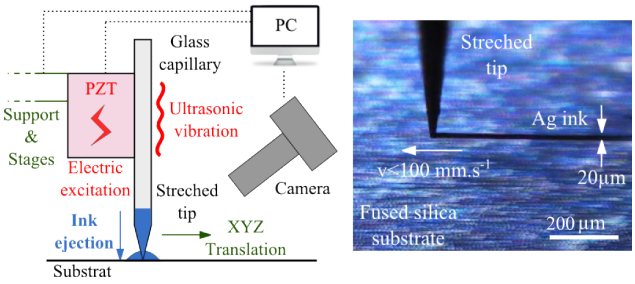

Figure 1: Illustration of the plotter printing (Microplotter II - Sonoplot). This printing method achieves resolutions ranging from 10 µm to 200 µm with standard conductive inks (5-15 cP).

After deposition, we used a hot plate to evaporate the solvent and metalize the nanoparticles. In the following, we mostly used two substrates, a flexible 3 µm thick polyethylene terephthalate (PET) film and a 50 µm thick fused silica (FS) wafers. As the melting temperature of PET (250 °C) is much lower than that of FS (1600 °C), structures printed on a PET substrate were heated to 220 °C for 30 minutes, while structures printed on FS were cured to 350 °C for 5 minutes. The scanning electron microscopy (SEM) images in figure 2 illustrate the coalescence of silver nanoparticles under thermal annealing for a single metal layer. An annealing temperature of 220 °C leads to weak sintering of the initial 10 nm diameter nanoparticles resulting in the formation of a weakly conductive metal layer. At 350 °C, the sintering is strong enough to cause the formation of a very rough metallic layer including agglomerates up to 1 µm in diameter. The conductivity was measured by using a four-terminal sensing method (SP4 Microworld) [53] with samples made up of a homogeneous 800 nm thick metal layer on an insulating substrate (SiO2 wafer) fabricated by spin coating. The values measured for the layer annealed at 220 °C (resp. 350 °C) was $6,0.10^6\ Sm^{-1}$ (resp. $16.10^6\ Sm^{-1}$), *i.e.* 10% of the conductivity of bulk silver (resp. 25%).

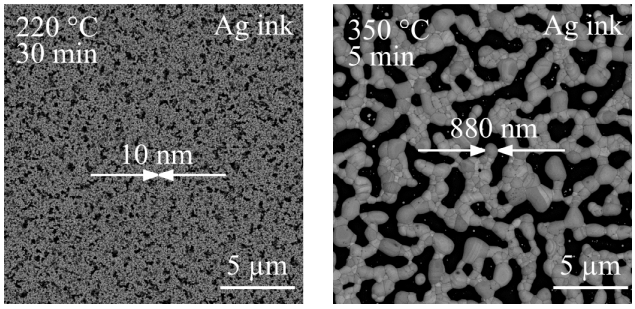

Figure 2: SEM images obtained with a TESCAN MIRA3 showing the metallization of an ink based on silver nanoparticles (JSA291 - Metalon) on PET substrate (left) and fused silica wafer (right) at different temperatures (220 °C, 30 min; resp. 350 °C, 5 min).

3. Glass tip optimization/Results

The glass tip is the central element of the process and need to be carefully designed to optimize the printing. We used a micropipette puller (P-1000, Sutter Instrument) to heat the initial glass capillary and separate it into two tips. By varying the conditions for stretching the glass (form and temperature of the heating element, stretching speed and acceleration, number of heating cycles, time and pressure of the cooling air...) we are able to produce a wide variety of tips to optimize its width according to the ink used and the desired resolution [54]. For example, increasing the pulling strength will lead to smaller apertures with longer tapers (see figure 3) which are more suitable for fluid inks. The type of glass (borosilicate or aluminosilicate) and the initial thickness and diameter of the capillary will also determine the proprieties of the tip. An aluminosilicate glass is more expensive, slightly more resistant to mechanical shocks but also more heat resistant leading to smaller taper at a fixed aperture size.

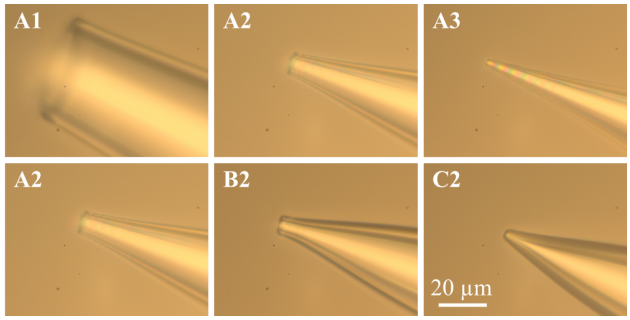

Figure 3: Microscope image of the glass tips made by stretching. The tips "A1", "A2" and "A3" illustrate the geometric variation of the aperture with the pulling speed (respectively +30% and +43%). The B2 and C2 tips are obtained from the A2 tip by fire-polishing for 60 and 75 ms respectively.

Experimentally, we observe that a shorter taper (< 3 mm) is better for reloading and ejecting the ink which is

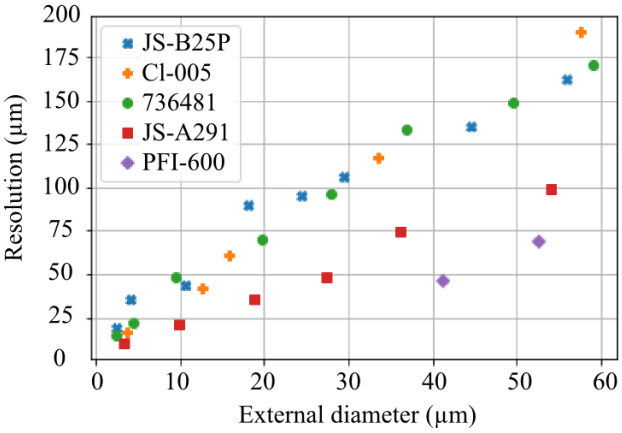

Figure 4: Print resolution obtained as a function of tip geometry for different commercial inks (see Table 1) on silicon substrate without excitation voltage.

Ink	Content (wt%)	Visc. (cP)	Solvent
JS-B25P	25 (Ag)	6.0	H_2O
Cl-005	27.5 (Cu)	11.9	H_2O
736481	30.2 (Ag)	12.1	$C_8H_{18}O_4$
JS-A291	40 (Ag)	8.3	H_2O
PFI-600	61.2 (Ag)	249	H_2O

Table 1: Commercial inks used for printing tests.

obtained by slow stretching of the capillary with many heating cycles (≈ 8). Moreover, with a wall less than a micron, the tip has a great chance of being crushed during the approaches. It is then necessary to slightly recast the end of the tip with a microforge in order to solidify it. Indeed, this process results in reducing the inner and outer diameter of the tip by retraction while increasing the thickness of the wall as shown in figure 3.

It is essential to finely optimize the printing parameters according to ink and capillaries to reach the expected resolution. In order to define the print parameters, we draw series of 2 mm lines on silicon with different glass tips and commercial inks designed for inkjet and even flexographic printing (see table 1) at ambient temperature and pressure, as shown in figure 4. For each ink concentration, composition or viscosity, the amount of fluid deposited depends linearly on the external diameter of the tip. For low concentrated inks, the ultimate resolution of this printing system is only limited by the fragility of the tips used (10 µm). On the contrary, for more viscous inks, the resolution is limited by the surface tension of the ink in the tip. As a result, flexographic inks cannot be easily used with tips smaller than 40 µm. The precision of the deposit and the possibility of printing viscous inks set plotter printing apart from more traditional inkjet printing systems.

It is also possible to tune the intensity of the excitation of the piezoelectric element to control the flow of ink that is deposited. Figure 5 shows the evolution of the width of a printed line for the same capillary with an external diameter of 10 µm as a function of the excitation voltage of the piezoelectric element. This evolution is exponential for relatively low voltages (0-5 V): it is thus possible to finely control the print resolution by about one order of magnitude using this parameter. This flexibility can lead to a significant reduction in printing time for complex patterns that require good spatial resolution in some areas and a large amount of ink in other areas. When using a more viscous ink or in order to unblock a clogged tip, high voltages (up to 12V) can be applied causing the tip to vibrate strongly when it comes into contact with the surface. In this case, relatively thick tips and a solid substrate should be used to avoid damage. The ejection and spread of the ink depends also on a large number of other parameters such as the nature of the substrate and its roughness, the presence of impurities, the composition of the atmosphere, the temperature, etc. For example, the surface energy of the substrate plays an important role in printing: the higher it is, the more the ink will tend to minimize its surface energy by forming thinner and thicker lines. Typical values for surface free energy are respectively: 66 mN/m, 55 mN/m and 43 mN/m for silicon, fused silica and PET [55, 56]. This is why, under identical experimental conditions and with the same ink (JS-A291) and the same tip, the thickness of the lines printed on silicon, sapphire or PET substrates may vary as shown in figure 5. It has been demonstrated that through physical, chemical or UV treatments, it is possible to modify the surface energy of the substrate in order to increase or decrease the wettability of the surface and therefore tune the resolution of the printing [57, 58, 59, 60].

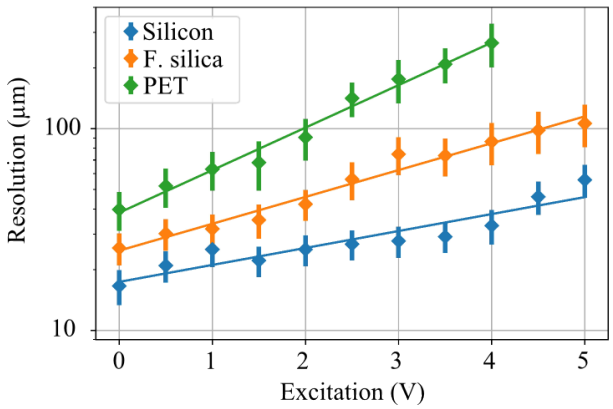

Figure 5: Variability in print resolution as a function of piezoelectric excitation and substrate type. The ink used was JS-A291 with a 10 µm outer diameter tip.

Finally, the printing speed is also a key parameter. Under otherwise equal experimental conditions, increasing the speed and acceleration of the mechanical arm reduces the print resolution by up to a factor of 3 as shown in figure 6(a) at the cost of the deposited thickness. The SEM images in figure 6(b) show the porosity of the metal layer after annealing (350 °C, 5 min) for two deposition speeds. This fill factor has been determined by image processing and appears to vary inversely exponentially with the printing speed as

shown in figure 6(c). As a result, the average cross-section of the deposited lines can be calculated by taking into account the line width, the average layer thickness and its fill factor (figure 6(d)). Two regimes can be distinguished: a first one, at low speed, where the ink can spread over an area larger than the tip diameter. Thus the resolution is mainly limited by the viscosity of the ink and the nature of the substrate. The second regime appears at high speed where the deposition is mainly limited by the ejection of the ink and for which the printing resolution reaches the outer diameter of the tip.

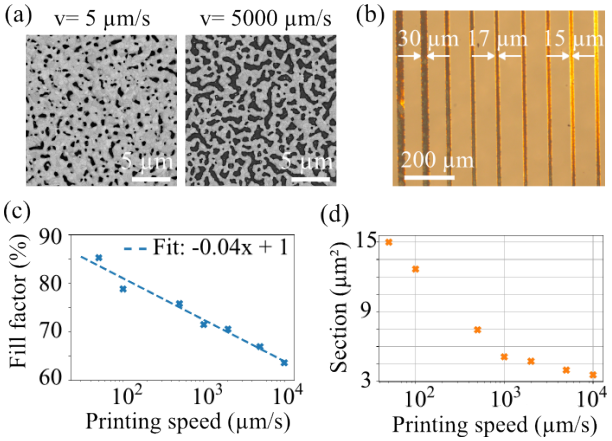

Figure 6: (a) Printed lines of JS-A291 on fused silica substrate observed under optical microscope: Print speed increases from left to right (5 µm/s to 10 mm/s). (b) SEM images of a metal layer after annealing at 350 °C during 5 min deposited respectively at 50 and 5000 µm/s on silicon substrate. (c) Fill factor measured from SEM images. (d) Calculated cross section of printed lines.

4. Fabrication of metasurfaces/Discussion

Two periodic arrays of metallic split ring resonators (SRR) have been printed on a very thin membrane of polyethylene terephthalate (PET, 3 µm - Goodfellow) and on a 60 µm thick fused silica wafer (Si-Mat). The SRRs frequency resonances have been tuned in the 60-80 GHz spectral domain. The resonant behavior of this well-known resonator is described in literature [61, 62, 63, 64]. Refractive indexes of PET and fused silica were measured by time domain spectroscopy (Menlo THz-TDS System): $n_{PET} = 1.65$ and $n_{FS} = 2.01$. The electromagnetic simulations of the resonators were carried out using the COMSOL software.

The PET was stuck by capillary adhesion to a silicon wafer in order to ensure flatness during printing. At maximum speed of 500 µm/s, the mean metal's thickness deposited by one print varies between 300 and 400 nm (see figure 7). To exceed the skin depth according to the conductivity values stated above, it is necessary to reach a metal's height of 726 nm on PET and 445 nm on fused silica at 80 GHz. We have then to iterate the print at least 3 times. A partial metallization of the ink by partial annealing (2 min at 120 °C) is necessary between each iteration to avoid clogging the tip. The graph of the figure 7(a) and the SEM images of the figure 7(b) show the evolution of the thickness of a metal layer as a function of the number of deposits for the two annealing temperatures on the two different substrates. For a low annealing temperature (T=220 °C), the thickness evolution is linear with the number of deposits. For a higher annealing temperature (T=350 °C), the second deposit fills the holes of the initial metal layer (see figure 2). The following deposits then increase the thickness of the layer until a porous layer is formed as shown in figure 2. For a total of 15 × 15 resonators with three successive printings superimposed, the manufacturing time was 3 hours (see figure 8). Variations in the manual re-positioning of the samples between each print result in a slight degradation of the reproducibility of the antennas which remains nevertheless remarkable for additive manufacturing: figure 8(b) shows that the printing dispersion for metasurfaces on PET and fused silica is less than 10 µm for both substrate types.

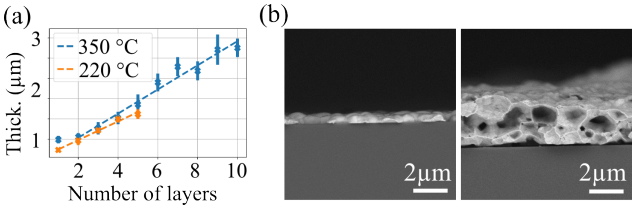

Figure 7: (a) Thickness of the metallic layer depending on the number of prints (annealed at 220 °C and 350 °C on fused silica substrate). (b) SEM images of a single (left) and ten successive metal layers (right) deposited on fused silica substrate.

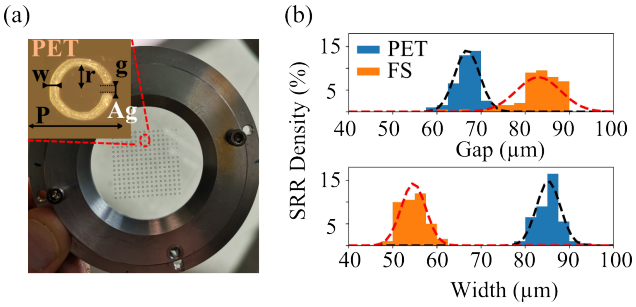

Figure 8: (a) Printed metasurface consisting of a periodic array of 15 × 15 SRR. (b) Dispersion of the fabrication on the gap (top) and the width (bottom) of the resonators. The dimensions on PET (resp. FS) are: P= 2000 µm, r=334 µm, g=83±5 µm and w=55±3 µm (resp. P= 1500 µm, r=252 µm, g=67±3 µm and w=85±3 µm)

To characterize the fabricated metasurfaces, we use a spectroscopic setup with homodyne detection illustrated on figure 9. A modulated and collimated terahertz source based on Schottky diodes (TeraSchottky, Lytid) illuminates the metasurface and the transmitted beam is collected by a terahertz pyrometer (TeraPyro, Lytid). The pyrometer is coupled to the source by a lock-in amplifier (SR830 Stan-

ford Research) that enables the extraction of the transmitted amplitude. By sweeping the frequency of the source we are then able to access the transmission spectra of the samples in the 60-80 GHz range.

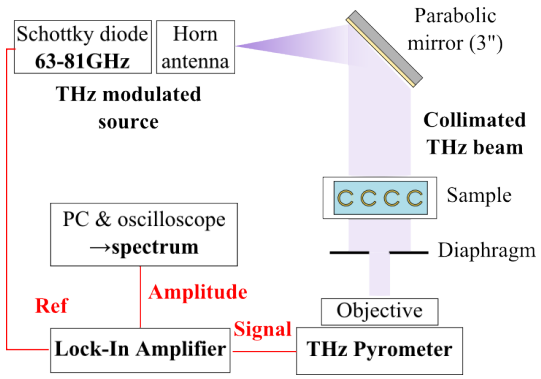

Figure 9: Scheme of the THz spectroscopic setup.

As expected in theory and simulations, the two printed metasurfaces present a transmission dip at about 70 GHz due to the inductive behavior of the SRR antennas (see fig 10). When a resonant magnetic flux penetrates the metal rings, it will induce rotating currents by Faraday's law which produce their own flux to oppose the incident field. In transverse magnetic (TM) polarisation, the electric field being perpendicular to the SRR gap, the electrons circulate throughout the entire ring, giving rise to a first resonant mode at around 70 GHz for the two fabricated samples. In transverse electric polarisation (TE), the electric field is parallel to the gap and the electrons circulate in half of the SRR, giving rise to a second resonant mode at around 150 GHz. Thus, with the described setup, only the first resonant mode is visible in TM polarisation. The quality factor ($Q = \lambda/\delta\lambda$) of SRR printed on fused silica is slightly higher than that printed on PET due to the higher conductivity of the metal layer.

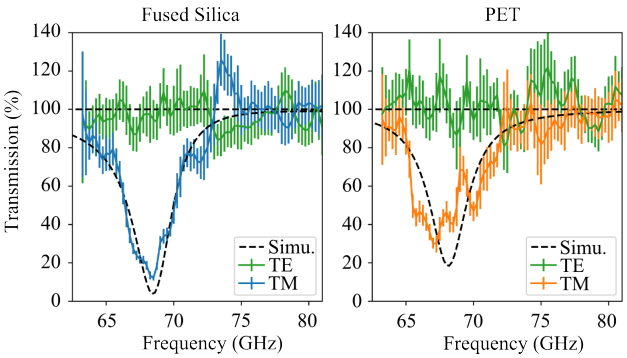

Figure 10: Transmission spectra of metasurfaces printed on PET and fused silica. The simulations were performed using the finite element simulation software COMSOL on a structure with periodic conditions in the xy plane.

5. Conclusion

We have demonstrated the fabrication of ultra-thin metasurfaces consisting of periodic arrays of resonant SRRs in the 60-80 GHz range with an ultrasonic excited printing system. The manufacturing method is fully described and optimized: it appears to be low cost and reproducible (dispersion $< 5\mu m$) even for flexible and fragile substrates. Substrates as thin as 3µm can be used, opening the way to new potential applications such as terhaertz imaging by thermoconversion [65]. As with all inkjet printing techniques, the limiting factor is the deposited metal thickness, particularly in the case of fine resolution which prevents the use of viscous inks. It is then recommended to make multiple prints using fast drying inks to exceed the skin thickness of the metal at the desired frequency. In addition, this printing technique can also be used for precision deposition of inks with other physico-chemical properties (graphene, h-BN, ZnO nanoparticles...) for the design of more complex THz resonators. The versatility, simplicity and reliability of the plotter printing make it a technology of choice in the field of precision printed electronics and is ideally suited for the fabrication of metasurfaces in the sub-terahertz and even terahertz domain, paving the way for rapid prototyping of terahertz components.

6. Acknowledgments

The authors would like to thank Amadine Andrieux and Frederic Fossard of the Laboratoire d'études des microstructures (LEM-ONERA-CNRS, Chatillon - FRANCE) for MEB measurements and the Agence de l'innovation de défense (AID - FRANCE) for their financial support.

Otherwise, the authors declare no conflicts of interest with respect to the content, authorship, and/or publication of this article.

References

[1] S. S. Dhillon, M. S. Vitiello, E. H. Linfield, A. G. Davies, Matthias C. Hoffmann, John Booske, Claudio Paoloni, M. Gensch, P. Weightman, G. P. Williams, E. Castro-Camus, D. R. S. Cumming, F. Simoens, I. Escorcia-Carranza, J. Grant, Stepan Lucyszyn, Makoto Kuwata-Gonokami, Kuniaki Konishi, Martin Koch, Charles A. Schmuttenmaer, Tyler L. Cocker, Rupert Huber, A. G. Markelz, Z. D. Taylor, Vincent P. Wallace, J. Axel Zeitler, Juraj Sibik, Timothy M. Korter, B. Ellison, S. Rea, P. Goldsmith, Ken B. Cooper, Roger Appleby, D. Pardo, P. G. Huggard, V. Krozer, Haymen Shams, Martyn Fice, Cyril Renaud, Alwyn Seeds, Andreas Stöhr, Mira Naftaly, Nick Ridler, Roland Clarke, John E. Cunningham, and Michael B. Johnston. The 2017 terahertz science and technology roadmap. *Journal of Physics D: Applied Physics*, 50(4):043001, January 2017.

[2] Ashish Y. Pawar, Deepak D. Sonawane, Kiran B. Erande, and Deelip V. Derle. Terahertz technology

and its applications. *Drug Invention Today*, 5(2):157–163, 2013.

[3] Xiang Yang, Xiang Zhao, Ke Yang, Yueping Liu, Yu Liu, Weiling Fu, and Yang Luo. Biomedical Applications of Terahertz Spectroscopy and Imaging. *Trends in Biotechnology*, 34(10):810–824, 2016.

[4] Withawat Withayachumnankul, Ryoumei Yamada, Masayuki Fujita, and T. Nagatsuma. All-dielectric rod antenna array for terahertz communications. *APL Photonics*, 3:051707, May 2018.

[5] Quanlong Yang, Jianqiang Gu, Dongyang Wang, Xueqian Zhang, Zhen Tian, Chunmei Ouyang, Ranjan Singh, Jiaguang Han, and Weili Zhang. Efficient flat metasurface lens for terahertz imaging. *Optics express*, 22 21:25931–9, 2014.

[6] Chun-Chieh Chang, Daniel Headland, Derek Abbott, Withawat Withayachumnankul, and Hou-Tong Chen. Demonstration of a highly efficient terahertz flat lens employing tri-layer metasurfaces. *Opt. Lett.*, 42(9):1867–1870, May 2017.

[7] Dandan Sun, Limei Qi, and Ziyu Liu. Terahertz broadband filter and electromagnetically induced transparency structure with complementary metasurface. *Results in Physics*, 16:102887, 2020.

[8] Hyeon Sang Bark, Geun Ju Kim, and Tae-In Jeon. Transmission characteristics of all-dielectric guided-mode resonance filter in the THz region. *Scientific Reports*, 8, 2018.

[9] Wenli Huang, Xiaoqing Luo, Yuanfu Lu, Fangrong Hu, and Guangyuan Li. Ultra-broadband terahertz bandpass filter with dynamically tunable attenuation based on a graphene–metal hybrid metasurface. *Appl. Opt.*, 60(22):6366–6370, August 2021.

[10] Hang Wong, Kai Xu Wang, Laure Huitema, and Aurelian Crunteanu. Active meta polarizer for terahertz frequencies. *Scientific Reports*, 10(1):15382, September 2020.

[11] Bin Lu, Haitao Wang, Jun Shen, Jun Yang, Hongyan Mao, Liangping Xia, Weiguo Zhang, Guodong Wang, Xiao-Yu Peng, and Deqiang Wang. A high extinction ratio THz polarizer fabricated by double-bilayer wire grid structure. *AIP Advances*, 6:025215, February 2016.

[12] Tetsuo Kan, Akihiro Isozaki, Natsuki Kanda, Natsuki Nemoto, Kuniaki Konishi, Hidetoshi Takahashi, Makoto Kuwata-Gonokami, Kiyoshi Matsumoto, and Isao Shimoyama. Enantiomeric switching of chiral metamaterial for terahertz polarization modulation employing vertically deformable MEMS spirals. *Nature Communications*, 6(1):8422, October 2015.

[13] Nian-Hai Shen, Maria Massaouti, Mutlu Gokkavas, Jean-Michel Manceau, Ekmel Ozbay, Maria Kafesaki, Thomas Koschny, Stelios Tzortzakis, and Costas M. Soukoulis. Optically Implemented Broadband Blueshift Switch in the Terahertz Regime. *Phys. Rev. Lett.*, 106(3):037403, January 2011.

[14] Hongyu Ji, Bo Zhang, Guocui Wang, Wei Wang, and Jingling Shen. Photo-excited multi-frequency terahertz switch based on a composite metamaterial structure. *Optics Communications*, 412:37–40, 2018.

[15] Longqing Cong, Prakash Pitchappa, Chengkuo Lee, and Ranjan Singh. Active Phase Transition via Loss Engineering in a Terahertz MEMS Metamaterial. *Advanced materials (Deerfield Beach, Fla.)*, 29, May 2017.

[16] Yue Wang, Dongying Zhu, Zijian Cui, Lisha Yue, Xiang Zhang, Lei Hou, Kuang Zhang, and Hui Hu. Properties and Sensing Performance of All-Dielectric Metasurface THz Absorbers. *IEEE Transactions on Terahertz Science and Technology*, 10(6):599–605, 2020.

[17] Amarveer Singh Dhillon and Divesh Mittal. Wide band ultrathin polarization insensitive electric field driven metamaterial absorber. *Optics Communications*, 443, March 2019.

[18] Fuli Zhang, Shuqi Feng, Kepeng Qiu, Zijun Liu, Yuancheng Fan, Weihong Zhang, Qian Zhao, and Ji Zhou. Mechanically Stretchable and Tunable Metamaterial Absorber. *Applied Physics Letters*, 106:091907, March 2015.

[19] Zhiyu Tan, Fei Fan, Dan Zhao, Yunyun Ji, Jierong Cheng, and Shengjiang Chang. High-Efficiency Terahertz Nonreciprocal One-Way Transmission and Active Asymmetric Chiral Manipulation Based on Magnetoplasmon/Dielectric Metasurface. *Advanced Optical Materials*, 9:2002216, March 2021.

[20] Meisam Askari, David A. Hutchins, Peter J. Thomas, Lorenzo Astolfi, Richard L. Watson, Meisam Abdi, Marco Ricci, Stefano Laureti, Luzhen Nie, Steven Freear, Ricky Wildman, Christopher Tuck, Matt Clarke, Emma Woods, and Adam T. Clare. Additive manufacturing of metamaterials: A review. *Additive Manufacturing*, 36:101562, 2020.

[21] Enrique Castro-Camus, Martin Koch, and Arturo Hernandez-Serrano. Additive manufacture of photonic components for the terahertz band. *Journal of Applied Physics*, 127:210901, June 2020.

[22] Bing Zhang, Yong-Xin Guo, Herbert Zirath, and Yue Ping Zhang. Investigation on 3-D-Printing Technologies for Millimeter- Wave and Terahertz Applications. *Proceedings of the IEEE*, 105(4):723–736, April 2017. Conference Name: Proceedings of the IEEE.

[23] S. Park, Y. Li, D. B. Fullager, S. Schöche, C. M. Herzinger, S. Lee, and T. Hofmann. Terahertz-frequency dielectric anisotropy in three-dimensional polymethacrylates fabricated by stereolithography. *Optics Letters*, 45(7):1982–1985, April 2020. Publisher: Optical Society of America.

[24] L. D. van Putten, J. Gorecki, E. Numkam Fokoua, V. Apostolopoulos, and F. Poletti. 3D-printed polymer antiresonant waveguides for short-reach terahertz applications. *Applied Optics*, 57(14):3953–3958, May 2018. Publisher: Optical Society of America.

[25] Daena Madhi, Asger Kjærgård Pedersen, and Peter Uhd Jepsen. Bi-aspheric singlet THz lenses free of spherical aberration. In *2020 45th International Conference on Infrared, Millimeter, and Terahertz Waves (IRMMW-THz)*, pages 1–1, November 2020. ISSN: 2162-2035.

[26] Behnam Mirzaei, José Silva, Y. Luo, X. Liu, Lei Wei, Darren Hayton, J.R. Gao, and C. Groppi. Efficiency of multi-beam Fourier phase gratings at 1.4 THz. *Optics Express*, 25:6581, March 2017.

[27] Yanzhang Lin, Haizi Yao, Xuewei Ju, Ying Chen, Shuncong Zhong, and Xiangfeng Wang. Free-standing double-layer terahertz band-pass filters fabricated by femtosecond laser micro-machining. *Optics Express*, 25(21):25125–25134, October 2017. Publisher: Optical Society of America.

[28] Alexandre Chícharo, Tatiana G. Rappoport, Chun-Da Liao, Jérôme Borme, Nuno M. R. Peres, and Pedro Alpuim. Superior ultra-transparent broadband terahertz polarizers by nanoimprint lithography. *arXiv:2102.10029 [cond-mat, physics:physics]*, February 2021. arXiv: 2102.10029.

[29] Mariia Zhuldybina, Xavier Ropagnol, Chloé Bois, Ricardo J. Zednik, and François Blanchard. Printing accuracy tracking with 2D optical microscopy and super-resolution metamaterial-assisted 1D terahertz spectroscopy. *npj Flexible Electronics*, 4(1):1–7, September 2020. Bandiera_abtest: a Cc_license_type: cc_by Cg_type: Nature Research Journals Number: 1 Primary_atype: Research Publisher: Nature Publishing Group Subject_term: Electrical and electronic engineering;Imaging and sensing Subject_term_id: electrical-and-electronic-engineering;imaging-and-sensing.

[30] Aydin Sadeqi, Hojatollah Rezaei Nejad, and Sameer Sonkusale. Low-cost metamaterial-on-paper chemical sensor. *Optics Express*, 25(14):16092–16100, July 2017. Publisher: Optical Society of America.

[31] Hichem Guerboukha, Hichem Guerboukha, Yasith Amarasinghe, Rabi Shrestha, Angela Pizzuto, Daniel M. Mittleman, and Daniel M. Mittleman. High-volume rapid prototyping technique for terahertz metallic metasurfaces. *Optics Express*, 29(9):13806–13814, April 2021. Publisher: Optical Society of America.

[32] Janghoon Park, Hyi Jae Kang, Kee-Hyun Shin, and Hyunkyoo Kang. Fast sintering of silver nanoparticle and flake layers by infrared module assistance in large area roll-to-roll gravure printing system. *Scientific Reports*, 6(1):34470, October 2016. Bandiera_abtest: a Cc_license_type: cc_by Cg_type: Nature Research Journals Number: 1 Primary_atype: Research Publisher: Nature Publishing Group Subject_term: Electronic properties and materials;Mechanical engineering Subject_term_id: electronic-properties-and-materials;mechanical-engineering.

[33] Arthur Salmon, Melanie Lavancier, Cyprien Brulon, Laure Coudrat, Baptiste Fix, Guillaume Ducournau, Romain Peretti, and Patrick Bouchon. Rapid prototyping of flexible terahertz metasurfaces using a microplotter. *Optics Express*, 29, February 2021.

[34] Dongju Lee, Hyuk-Kee Sung, and Sungjoon Lim. Flexible subterahertz metamaterial absorber fabrication using inkjet printing technology. *Applied Physics B*, 122(7):206, July 2016.

[35] Bo-Cin Huang and Cheng-Yao Lo. Inkjet-Patterned Porous Split-Ring Resonator and Its Performance Study on Metamaterial Application. *Journal of Micromechanics and Microengineering*, 28, May 2018.

[36] Markus Walther, Alex Ortner, Henning Meier, Ute Löffelmann, Patrick J. Smith, and Jan G. Korvink. Terahertz metamaterials fabricated by inkjet printing. *Applied Physics Letters*, 95(25):251107, December 2009. Publisher: American Institute of Physics.

[37] K. Kashiwagi, L. Xie, X. Li, T. Kageyama, M. Miura, H. Miyashita, J. Kono, and S.-S. Lee. Flexible and stackable terahertz metamaterials via silver-nanoparticle inkjet printing. *AIP Advances*, 8(4):045104, April 2018. Publisher: American Institute of Physics.

[38] Asada Harumi, Kota Endo, Takehito Suzuki, and Takehito Suzuki. Reflectionless metasurface with high refractive index in the terahertz waveband. *Optics Express*, 29(10):14513–14524, May 2021. Publisher: Optical Society of America.

[39] Yeongjun Kim, Shin Jang, and Je Hoon Oh. High-resolution electrohydrodynamic printing of silver nanoparticle ink via commercial hypodermic needles. *Applied Physics Letters*, 106(1):014103, January 2015. Publisher: American Institute of Physics.

[40] Ayodya Tenggara, Saejune Park, Hadi Yudistira, Y Ahn, and Doyoung Byun. Fabrication of terahertz metamaterials using electrohydrodynamic jet printing

for sensitive detection of yeast. *Journal of Micromechanics and Microengineering*, 27:035009, February 2017.

[41] Keisuke Takano, Taku Kawabata, Cho-Fan Hsieh, Koichi Akiyama, Fumiaki Miyamaru, Yuji Abe, Yasunori Tokuda, Ru-Pin Pan, Ci-Ling Pan, and Masanori Hangyo. Fabrication of Terahertz Planar Metamaterials Using a SuperFine Ink-Jet Printer. *Applied Physics Express - APPL PHYS EXPRESS*, 3, January 2010.

[42] Christopher Oakley, Amanpreet Kaur, Jennifer A. Byford, and Premjeet Chahal. Aerosol-Jet Printed Quasi-Optical Terahertz Filters. In *2017 IEEE 67th Electronic Components and Technology Conference (ECTC)*, pages 248–253, May 2017. ISSN: 2377-5726.

[43] N. J. Wilkinson, M. A. A. Smith, R. W. Kay, and R. A. Harris. A review of aerosol jet printing—a non-traditional hybrid process for micro-manufacturing. *The International Journal of Advanced Manufacturing Technology*, 105(11):4599–4619, December 2019.

[44] David Jahn, Ralph Eckstein, Lorenz Schneider, Norman Born, Gerardo Hernandez-Sosa, Jan Balzer, Ibraheem Al-Naib, Uli Lemmer, and Martin Koch. Digital Aerosol Jet Printing for the Fabrication of Terahertz Metamaterials. *Advanced Materials Technologies*, 3, December 2017.

[45] Bradley J. Larson, Susan D. Gillmor, and Max G. Lagally. Controlled deposition of picoliter amounts of fluid using an ultrasonically driven micropipette. *Review of Scientific Instruments*, 75(4):832–836, April 2004. Publisher: American Institute of Physics.

[46] Xinda Wang, Wei Guo, Ying Zhu, Xiaokang Liang, Fude Wang, and Peng Peng. Electrical and Mechanical Properties of Ink Printed Composite Electrodes on Plastic Substrates. *Applied Sciences*, 8(11):2101, November 2018. Number: 11 Publisher: Multidisciplinary Digital Publishing Institute.

[47] Zhigang Zang, Xiaosheng Tang, Xianming Liu, Xiaohua Lei, and Weiming Chen. Fabrication of high quality and low cost microlenses on a glass substrate by direct printing technique. *Applied Optics*, 53(33):7868–7871, November 2014. Publisher: Optical Society of America.

[48] Jinyang Zhao, Yongli Yan, Zhenhua Gao, Yuxiang Du, Haiyun Dong, Jiannian Yao, and Yong Sheng Zhao. Full-color laser displays based on organic printed microlaser arrays. *Nature Communications*, 10(1):870, February 2019. Bandiera_abtest: a Cc_license_type: cc_by Cg_type: Nature Research Journals Number: 1 Primary_atype: Research Publisher: Nature Publishing Group Subject_term: Displays;Micro-optics Subject_term_id: displays;micro-optics.

[49] Le Cai, Suoming Zhang, Jinshui Miao, Zhibin Yu, and Chuan Wang. Fully Printed Stretchable Thin-Film Transistors and Integrated Logic Circuits. *ACS Nano*, 10(12):11459–11468, December 2016. Publisher: American Chemical Society.

[50] Chenning Liu, Hang Zhou, Qian Wu, Fuhua Dai, Tsz-Ki Lau, Xinhui Lu, Tengzhou Yang, Zixin Wang, Xuying Liu, and Chuan Liu. Guided Formation of Large Crystals of Organic and Perovskite Semiconductors by an Ultrasonicated Dispenser and Their Application as the Active Matrix of Photodetectors. *ACS Applied Materials & Interfaces*, 10(46):39921–39932, November 2018. Publisher: American Chemical Society.

[51] Adam P. Robinson, Ivan Minev, Ingrid M. Graz, and Stéphanie P. Lacour. Microstructured Silicone Substrate for Printable and Stretchable Metallic Films. *Langmuir*, 27(8):4279–4284, April 2011. Publisher: American Chemical Society.

[52] Xiaochen Fang, Jialin Shi, Xiujuan Zhang, Xiaobin Ren, Bei Lu, Wei Deng, Jiansheng Jie, and Xiaohong Zhang. Patterning Liquid Crystalline Organic Semiconductors via Inkjet Printing for High-Performance Transistor Arrays and Circuits. *Advanced Functional Materials*, 31(21):2100237, 2021. _eprint: https://onlinelibrary.wiley.com/doi/pdf/10.1002/adfm.202100237.

[53] Mariia Zhuldybina, Xavier Ropagnol, Charles Trudeau, Martin Bolduc, Ricardo J. Zednik, and François Blanchard. Contactless In Situ Electrical Characterization Method of Printed Electronic Devices with Terahertz Spectroscopy. *Sensors*, 19(3):444, January 2019. Number: 3 Publisher: Multidisciplinary Digital Publishing Institute.

[54] M. H. T. Roberts. Advanced Micropipette Techniques For Cell Physiology. *Journal of Anatomy*, 153:260–261, August 1987.

[55] D. K. Owens and R. Wendt. Estimation of the surface free energy of polymers. 1969.

[56] D. H. Kaelble. Dispersion-Polar Surface Tension Properties of Organic Solids. *The Journal of Adhesion*, 2(2):66–81, April 1970. Publisher: Taylor & Francis _eprint: https://doi.org/10.1080/0021846708544582.

[57] J. Park, Jong Sik Oh, E. Gil, S. Kyoung, J. Lim, and G Yeom. Polyimide Surface Treatment by Atmospheric Pressure Plasma for Metal Adhesion. *Journal of The Electrochemical Society*, 157, January 2010.

[58] Michael Noeske, Jost Degenhardt, Silke Strudthoff, and Uwe Lommatzsch. Plasma jet treatment of five

polymers at atmospheric pressure: surface modifications and the relevance for adhesion. *International Journal of Adhesion and Adhesives*, 24(2):171–177, April 2004.

[59] Alessandro Chiolerio, Paola Rivolo, Samuele Porro, Stefano Stassi, Serena Ricciardi, Pietro Mandracci, Giancarlo Canavese, Katarzyna Bejtka, and Candido Fabrizio Pirri. Inkjet-printed PEDOT:PSS electrodes on plasma-modified PDMS nanocomposites: quantifying plasma treatment hardness. *RSC Advances*, 4(93):51477–51485, October 2014. Publisher: The Royal Society of Chemistry.

[60] F. Ely, C. O. Avellaneda, P. Paredez, V. C. Nogueira, T. E. A. Santos, V. P. Mammana, C. Molina, J. Brug, G. Gibson, and L. Zhao. Patterning quality control of inkjet printed PEDOT:PSS films by wetting properties. *Synthetic Metals*, 161(19):2129–2134, October 2011.

[61] J.B. Pendry, Anthony Holden, D.J. Robbins, and W.J. Stewart. Magnetism from Conductors, and Enhanced Non-linear Phenomena. *Microwave Theory and Techniques, IEEE Transactions on*, 47:2075–2084, December 1999.

[62] D. R. Smith, Willie J. Padilla, D. C. Vier, S. C. Nemat-Nasser, and S. Schultz. Composite Medium with Simultaneously Negative Permeability and Permittivity. *Physical Review Letters*, 84(18):4184–4187, May 2000. Publisher: American Physical Society.

[63] Anders Pors, Morten Willatzen, Ole Albrektsen, and Sergey I. Bozhevolnyi. From plasmonic nanoantennas to split-ring resonators: tuning scattering strength. *JOSA B*, 27(8):1680–1687, August 2010. Publisher: Optical Society of America.

[64] J.D. Baena, J. Bonache, F. Martin, R.M. Sillero, F. Falcone, T. Lopetegi, M.A.G. Laso, J. Garcia-Garcia, I. Gil, M.F. Portillo, and M. Sorolla. Equivalent-circuit models for split-ring resonators and complementary split-ring resonators coupled to planar transmission lines. *IEEE Transactions on Microwave Theory and Techniques*, 53(4):1451–1461, April 2005. Conference Name: IEEE Transactions on Microwave Theory and Techniques.

[65] Arthur Salmon and Patrick Bouchon. Rapid prototyping of a bispectral terahertz-to-infrared converter. *Optics Express*, 29(12):18437–18445, June 2021. Publisher: Optical Society of America.